© 2020. Published by The Company of Biologists Ltd | Journal of Cell Science (2020) 133, jcs232264. doi:10.1242/jcs.232264

RESEARCH ARTICLE

Pushing myelination – developmental regulation of myosin expression drives oligodendrocyte morphological differentiation

Helena Sofia Domingues[1,2,3,*], Mateusz M. Urbanski[4], Sandra Macedo-Ribeiro[2,3], Amr Almaktari[4], Azka Irfan[4], Yamely Hernandez[4], Haibo Wang[4], João Bettencourt Relvas[2,3], Boris Rubinstein[5], Carmen V. Melendez-Vasquez[4,6,‡] and Inês Mendes Pinto[1,‡]

ABSTRACT

Oligodendrocytes are the central nervous system myelin-forming cells providing axonal electrical insulation and higher-order neuronal circuitry. The mechanical forces driving the differentiation of oligodendrocyte precursor cells into myelinating oligodendrocytes are largely unknown, but likely require the spatiotemporal regulation of the architecture and dynamics of the actin and actomyosin cytoskeletons. In this study, we analyzed the expression pattern of myosin motors during oligodendrocyte development. We report that oligodendrocyte differentiation is regulated by the synchronized expression and non-uniform distribution of several members of the myosin network, particularly non-muscle myosins 2B and 2C, which potentially operate as nanomechanical modulators of cell tension and myelin membrane expansion at different cell stages.

This article has an associated First Person interview with the first author of the paper.

KEY WORDS: Myosinome, Oligodendrocyte differentiation, Myelination, Cell tension, Membrane expansion

INTRODUCTION

Myelinating oligodendrocytes (OLs) are highly specialized cells of the vertebrate central nervous system (CNS) (Zalc, 2016). OLs derive from oligodendrocyte precursor cells (OPCs), which during differentiation protrude multiple hybrid (actin and tubulin-enriched) structures that further evolve into lamellipodia-like membranous extensions from which compact myelin is ultimately formed (Song et al., 2001; Wilson and Brophy, 1989; Domingues et al., 2018). Recent experimental evidence suggests that the remarkable morphological and functional transformations underlying OPC differentiation are driven by actin cytoskeleton-based forces (Kippert et al., 2009; Nawaz et al., 2015; Zuchero et al., 2015). In higher eukaryotes, the intrinsic dynamics of actin cytoskeleton is modulated by the presence of myosin motors. Humans display the highest number and classes of myosins, with almost 40 myosins distributed over 18 classes based on their sequence similarity. Such remarkable myosin variability supports its involvement in multiple and essential functions (e.g. cell differentiation, migration and division) (Sellers, 2000; Sebé-Pedrós et al., 2014; Heissler and Sellers, 2016). Structurally, myosins are characterized by three canonical domains: the motor domain with ATPase activity involved in actin binding and movement, the neck domain that binds myosin light chains and calmodulin, and a tail domain of variable length and class-specific composition that serves to anchor and position the motor domain so that it can interact with actin and connect to various cargo-associated proteins (Sellers, 2000).

The conventional non-muscle class II myosins (NM2) are hexameric structures composed of two heavy chains and two pairs of light chains [the regulatory light chain (RLC), and the essential light chain (ELC)]. The most striking characteristic of these myosins is their two-headed structure due to the dimerization of the heavy chain in the tail region to form bipolar filaments. These characteristics favor cell contractility when bound to and sliding on antiparallel actin filaments (Billington et al., 2013). In mammals there are three genes – *Myh9*, *Myh10* and *Myh14* – encoding the NM2 heavy chains. The heavy chains, together with the bound RLCs and ELCs, are termed NM2A, NM2B, and NM2C, respectively. In contrast, the unconventional class 1, class 5 and class 6 myosins do not form bipolar filaments and work in monomers or dimers to transport cargo (Li et al., 2016).

Several members of the myosin superfamily are known to be expressed by OLs and contribute to the process of myelination: the conventional NM2A and NM2B, and the unconventional myosin-1D (Myo1d), myosin-5A (Myo5a) and myosin-6 (Myo6). While NM2B function is associated with actomyosin contractility and we previously showed that its depletion in OLs accelerates myelination (Wang et al., 2008, 2012; Kippert et al., 2009; Rusielewicz et al., 2014), inhibition of myosins functionally associated with trafficking mechanisms, such as Myo1d, Myo5a or Myo6, lead to OL differentiation arrest (Sloane and Vartanian, 2007; Yamazaki et al., 2014, 2016, 2017). Despite this experimental evidence, it remains elusive how different myosins dynamically interplay and contribute to large-scale cellular behaviors during OL morphogenesis and myelination.

In this study, we conducted a systems biology-oriented analysis of the subcellular distribution of the OL myosinome, which included: (1) transcriptomic and proteomic databases, (2) myosin domain organization, (3) myosin mechanochemical properties, (4) functional enrichment of myosin interactomes, and (5) quantitative imaging of myelinating co-cultures of OLs with dorsal root ganglion (DRG) neurons depleted of specific isoforms of NM2 myosins. Our analysis reveals that the OL differentiation program is regulated by spatiotemporal synchronization of different myosins

[1]International Iberian Nanotechnology Laboratory (INL), 4715-330 Braga, Portugal. [2]Instituto de Investigação e Inovação em Saúde (I3S), Universidade do Porto, 4200-135 Porto, Portugal. [3]Instituto de Biologia Molecular e Celular (IBMC), Universidade do Porto, 4200-135 Porto, Portugal. [4]Department of Biological Sciences, Hunter College City University of New York, New York, NY 10065, USA. [5]Stowers Institute for Medical Research, Kansas City, MO 64110, USA. [6]The Graduate Center, City University of New York (CUNY), New York, NY 10016, USA.
*Present address: Life and Health Sciences Research Institute (ICVS), School of Medicine, University of Minho, 4710-057 Braga, Portugal.

‡Authors for correspondence (melendez@genectr.hunter.cuny.edu; ines.m.pinto@inl.int)

A.A., 0000-0002-1292-6818; A.I., 0000-0002-3603-3918; Y.H., 0000-0002-1356-4230; H.W., 0000-0002-0375-038X; I.M.P., 0000-0002-8009-7767

Handling Editor: Giampietro Schiavo
Received 22 March 2019; Accepted 24 June 2020

Journal of Cell Science (2020) 133, jcs232264. doi:10.1242/jcs.232264

able to modulate distinctive mechanical features. We hypothesize that, at early stages of OPC differentiation, cell symmetry breaking and emergence of local protrusions requires non-uniform cortical tension, which are dependent on NM2B topology. The transition to mature OL implies a global decrease of NM2B expression for cortical tension reduction and protrusive membrane growth. At this stage, NM2C could potentially contribute to vesicular transport promoting myelin membrane extension.

RESULTS

The myosinome of developing OLs – transcriptomic and proteomic datasets reveal contrasting temporal expression patterns

We aimed to identify and catalog all myosins expressed in developing OL and establish how their expression temporally correlates with the different stages of differentiation. Combined expression analysis (transcriptomic and proteomic data) (Cahoy et al., 2008; Wang et al., 2008; De Monasterio-Schrader et al., 2012; Zhang et al., 2014; Marques et al., 2016; Thakurela et al., 2016; Yamazaki et al., 2017; Azevedo et al., 2018) identified 16 myosins in the OL lineage belonging to classes 1, 2, 5, 6, 9, 10, 16, 18 and 19: Myo1b, Myo1c, Myo1d, Myo1e, Myo1f, Myh9, Myh10, Myh14, Myo5a, Myo6, Myo9a, Myo9b, Myo10, Myo16, Myo18a and Myo19. Among these, seven were consistently identified in five independent studies: Myo1d, Myh9, Myh10, Myh14, Myo5a, Myo6 and Myo18a (Fig. 1A). Analysis of myosin transcript abundances and expression profiles, as reported in the Brain RNASeq (http://www.brainrnaseq.org; Zhang et al., 2014), clearly shows that seven myosins are developmentally regulated and display two contrasting expression profiles. Specifically, *Myh9*, *Myh10* and *Myo5a* are markedly downregulated during OL differentiation, while the expression of *Myo1d*, *Myh14*, *Myo6* and *Myo18a* transcripts is upregulated (Fig. 1B). Of note, OLs express all the three transcripts for the heavy chains of conventional non-muscle class 2 myosin isoforms – *Myh9*, *Myh10* and *Myh14*. In agreement with our previous published data (Wang et al., 2008), we observe the expression of NM2A (*Myh9*) and NM2B (*Myh10*) transcripts in the OL lineage and their decreased protein expression during differentiation (Fig. 1C). By contrast, we observe that the transcript for NM2C (*Myh14*) heavy chain as well as its protein levels have an opposite expression profile, that is, increased expression during OL differentiation (Fig. 1A–C). Interestingly, myosin Myo18a, which is phylogenetically related to NM2s (Peckham, 2011), is also upregulated in myelinating OLs (Fig. 1A–C). The same pattern of expression, that is, decreased for NM2B and increased for NM2C as myelination proceeds, is observed in developing rat brain (Fig. S1). These findings are confirmed by the enrichment of NM2C and Myo18a in the transcriptome and proteome of purified CNS myelin fractions of both rodent and human origin (Cahoy et al., 2008; De Monasterio-Schrader et al., 2012), and in agreement with earlier evidence of higher abundance of *Myh14* transcripts in human adult tissues, especially in white matter-enriched regions (Golomb et al., 2004). Unlike *Myh9* and *Myh10*, *Myh14* is not expressed in mouse embryonic stem cells or fetal tissues (Golomb et al., 2004). At the subcellular level, we have previously observed that *Myh14* and *Myo18a* mRNAs are significantly enriched in OPC protrusions (Fig. 1A) (Azevedo et al., 2018). Although the physiological significance of such enrichment is still unknown, OPC protrusions are important structures for cell branching, local regulation of myelin basic protein (MBP) translation and membrane expansion during myelination (Laursen et al., 2011; Azevedo et al., 2018). Protein expression of the unconventional myosins Myo1d, Myo5a and Myo6 was recently analyzed in developing rat OL cultures (Fig. 1A) (Yamazaki et al., 2017). While increased Myo1d expression during OL differentiation was detected in that study at both the protein and mRNA, the levels of Myo5a and Myo6 proteins levels do not change during OL differentiation. Altogether, the expression analyses of the different myosins in developing OLs indicate that the myosinome is temporally regulated, in particular the three known isoforms of non-muscle class 2 myosins (NM2A, NM2B and NM2C) and their closest relative Myo18a.

The phylogenetically and structurally related NM2A, NM2B, NM2C and Myo18a myosins have distinct mechanochemical profiles

In order to understand the functional relevance of contrasting expression profiles of transcripts encoding the four phylogenetically related NM2A, NM2B, NM2C and Myo18a proteins in developing OLs (Peckham, 2011), we conducted a careful re-evaluation of their structural protein domain organization. Combining the information available in UniProt (https://www.uniprot.org) and Pfam databases (https://pfam.xfam.org), we retrieved the data on the conserved domains and functional sites of NM2A, NM2B, NM2C and Myo18a (Fig. 2A), and confirmed that overall there are no significant differences in the domain organization of the three NM2 isoforms. When compared with Myo18a, the tail domain of class 2 and 18 myosins have a similar α-helical coiled-coil region of comparable size, one IQ calmodulin-binding site that binds the ELC and RLC in the neck domain, and one myosin-N-terminal SH3-like region in the motor domain. However, in the motor domain, Myo18a has three other regions that clearly distinguishes it from the three NM2 isoforms. First, Myo18a lacks the canonical 23-amino-acid sequence actin-binding region in the myosin head domain. Instead, Myo18a has a 5-amino-acid sequence actin-binding region outside the myosin head domain that is ATP independent. Also, upstream in its N-terminus, Myo18a has a KE-rich region. Finally, downstream from the KE-rich region, this myosin has a PDZ domain, which is known to be involved in protein–protein interactions (Furusawa et al., 2000; Isogawa et al., 2005).

In addition to mRNA expression profiles and protein structural domains, the different myosin functions can also be explained by mechanochemical properties including: (1) the enzymatic activity of the motor domains that enables its processivity along the actin filaments, (2) the isoform-specific heavy chain phosphorylation by upstream regulators, and (3) interactions with proteins that may regulate myosin filament assembly and its activity upon actin binding (Clark et al., 2007, 2008; Tan et al., 2008; Heissler and Sellers, 2016; Melli et al., 2018). We have summarized what is currently known about the bipolar myosin filaments structure and the mechanochemical properties of these four myosins (Fig. 2B) (Billington et al., 2013, 2015). All form homotypic antiparallel bipolar filaments, but NM2s have longer coiled-coil tails compared to those of Myo18a and form longer myosin filaments. Additionally, there are other relevant differences in filament structure, enzymatic properties and actin binding behavior among the three NM2 isoforms. Specifically, NM2A and NM2B share more common features when compared with NM2C and Myo18a: NM2A and NM2B have higher ATPase motor activity ($0.41\ s^{-1}$, $0.23\ s^{-1}$ and $0.13\ s^{-1}$ for NM2A, NM2B and NM2C, respectively), larger filament width (11.2 nm, 11.5 nm and 7.9 nm for NM2A, NM2B and NM2C, respectively) (Billington et al., 2013) and contain higher number of myosin molecules per filament (29, 30 and 14 for NM2A, NM2B and NM2C, respectively) (Billington et al., 2013). By contrast, NM2C has a longer bare zone (M-region) (167 nm, 166 nm and 219 nm for NM2A, NM2B and NM2C, respectively) (Billington et al., 2013). This suggests that NM2C may form bipolar

Journal of Cell Science (2020) 133, jcs232264. doi:10.1242/jcs.232264

A

The oligodendrocyte Myosinome

Gene ID	Protein name	*In vivo* CNS myelin (tissue global)		*Ex vivo* and *in vitro* Oligodendrocte differentiation (cell-global)				*In vitro* OPC protrusiosome (cell-local)
		Transcriptomics RNAseq (Thakurela et al 2016) NCBI-GEO GSE 78151	Proteomics meta-analysis (deMonasterio-Schrader et al 2012)	Transcriptomics Microarray (Cahoy et al 2008) NCBI-GEO GSE 9566	Transcriptomics Bulk RNAseq (Zhang et al 2014) NCBI-GEO GSE 52564	Transcriptomics Single cell RNAseq (Marques et al 2016) NCBI-GEO GSE75330	Western blot	Transcriptomics Bulk RNAseq (Azevedo et al 2018) NCBI-GEO GSE 9566
Myo1b	Myosin 1b	-	-	Down-regulation	Down-regulation	Down-regulation	-	-
Myo1c	Myosin 1c	-	-	Down-regulation	Down-regulation	Down-regulation	-	-
Myo1d	**Myosin 1d**	**Present in CNS myelin**	**Present in CNS myelin**	**Up-regulation**	**Up-regulation**	**Up-regulation**	**Up-regulation (Yamazaki et al 2017)**	-
Myo1e	Myosin 1e	Present in CNS myelin	-	Up-regulation	Up-regulation	Up-regulation	-	-
Myo1f	Myosin 1f	-	-	-	Down-regulation	Down-regulation	-	-
Myh9	**Non-muscle myosin 2a (NM2A)**	**Present in CNS myelin**	**Present in CNS myelin**	**Unchanged-low**	**Down-regulation**	**Variable**	**Down-regulation (Wang et al 2012)**	-
Myh10	**Non-muscle myosin 2b (NM2B)**	**Present in CNS myelin**	**Present in CNS myelin**	**Down-regulation**	**Down-regulation**	**Down-regulation**	**Down-regulation (Wang et al 2012)**	-
Myh14	**Non-muscle myosin 2c (NM2C)**	**Present in CNS myelin**	**Present in CNS myelin**	**Up-regulation**	**Up-regulation**	**Up-regulation**	-	**Enriched in OPC protrusions**
Myo5a	**Myosin 5a**	**Present in CNS myelin**	**Present in CNS myelin**	**Down-regulation**	**Down-regulation**	**Down-regulation**	**Unchanged (Yamazaki et al 2017)**	-
Myo6	**Myosin 6**	**Present in CNS myelin**	**Present in CNS myelin**	**Up-regulation**	**Up-regulation**	**Up-regulation**	**Unchanged (Yamazaki et al 2017)**	**Enriched in OPC protrusions**
Myo9a	Myosin 9a	-	-	Up-regulation	Down-regulation	Up-regulation	-	-
Myo9b	Myosin 9b	-	-	Up-regulation	Down-regulation	Up-regulation	-	-
Myo10	Myosin 10	-	-	Down-regulation	Down-regulation	Down-regulation	-	-
Myo16	Myosin 16	-	-	-	Down-regulation	-	-	-
Myo18a	**Myosin 18a**	**Present in CNS myelin**	**Present in CNS myelin**	**Up-regulation**	**Up-regulation**	**Up-regulation**	-	**Enriched in OPC protrusions**
Myo19	Myosin 19	-	-	-	Down-regulation	Down-regulation	-	-

B

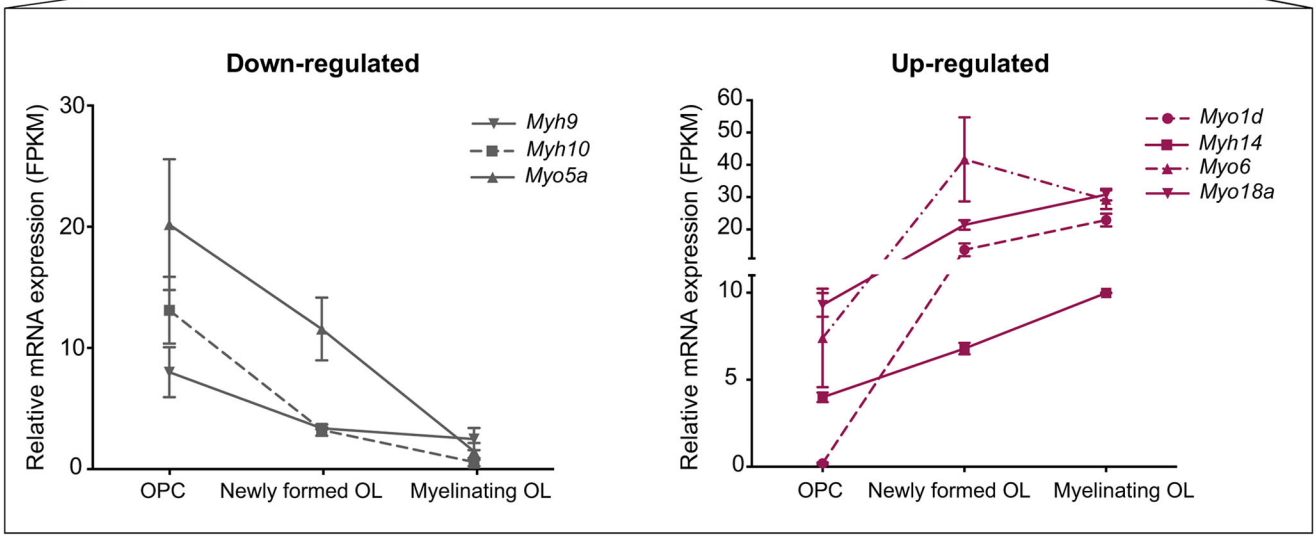

C

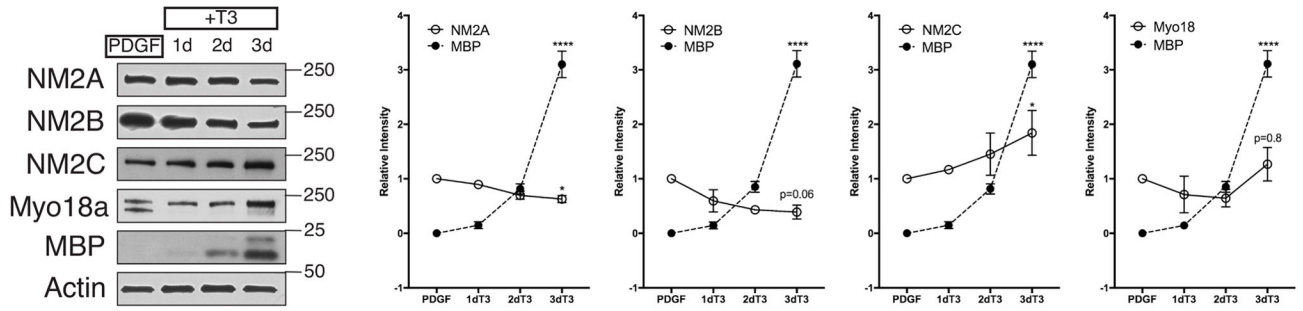

Fig. 1. See next page for legend.

Journal of Cell Science (2020) 133, jcs232264. doi:10.1242/jcs.232264

Fig. 1. The myosinome of developing OLs – transcriptomic and proteomic datasets reveal contrasting temporal expression patterns. (A,B) Data mining for the mRNA and protein spatiotemporal expression profile of the different members of the myosin network during OL differentiation. This information was collected from available *in vitro*, *ex vivo* and *in vivo* high-throughput transcriptomic and proteomic datasets or specific studies in human, mouse and rat. It reports the presence of specific myosins in myelinated fractions isolated from *in vivo* CNS tissue, at the mRNA and protein levels (De Monasterio-Schrader et al., 2012; Thakurela et al., 2016). Also, it describes quantitatively the temporal expression pattern for mRNA and protein during different stages of *ex vivo* and *in vitro* OL differentiation (unchanged, upregulated or downregulated) (Cahoy et al., 2008; Wang et al., 2012; Zhang et al., 2014; Marques et al., 2016; Yamazaki et al., 2017). Finally, it identifies myosin mRNAs subcellularly enriched in OPC protrusions (Azevedo et al., 2018). In light gray are highlighted seven myosins consistently identified in several studies: Myo1d, Myh9, Myh10, Myh14, Myo5a, Myo6 and Myo18a. Their transcript expression profiles during different stages of mouse OL differentiation (OPC, newly formed OL and myelinating OL) are graphically represented for one of the studies (Zhang et al., 2014; http://www.brainrnaseq.org) (B). These were reported as fragments per kilobase of transcript sequence per million mapped fragments (FPKM) and plotted according to their expression pattern during OL differentiation: mRNA expression of *Myh9*, *Myh10* and *Myo5a* is markedly down-regulated (left graph), while the expression of *Myo1d*, *Myh14*, *Myo6* and *Myo18a* transcripts is up-regulated (right graph). Data are presented as mean±s.e.m. of two replicates of pooled animals for each cell type, according to Zhang et al., 2014. (C) Western blot from OPCs (PDGF condition) and OL under differentiation (days 1, 2 and 3 after differentiation in T3-containing medium) showing the correlation between protein levels of NM2A, NM2B (downregulation) and NM2C, Myo18a (up-regulation) and MBP protein expression. Data in graphs represent the ratio of each protein relative to actin band (mean±s.e.m.; from three lysates). Myosin ratios were normalized to the baseline PDGF value. *$P<0.05$; ****$P<0.0001$ [Krustal–Wallis non-parametric test followed by Dunn's multiple comparison (PDGF vs 3dT3)].

filaments with fewer component molecules. Additionally, NM2C has been previously described to differ from NM2A and NM2B in its binding capacity to actin (Fig. 2C) (Billington et al., 2013). The percentage of NM2C bipolar filaments that are not bound to actin is much higher than those of NM2A and NM2B, and the actin-bound NM2C structures are mainly characterized by a single actin filament attached to the myosin filament via one side only, while a higher proportion of NM2A and NM2B filaments associate more frequently to assembled actin and, most importantly, with more stable engagements (Fig. 2C). Altogether, the structure and mechanochemical properties of NM2A and NM2B are very similar but differ significantly from those of NM2C and Myo18a. The higher ATPase activity and number of myosin heads in NM2A and NM2B filaments, along with more stable engagements with actin determine their processivity along actin filaments (Stam et al., 2015; Melli et al., 2018), suggesting that they may be more capable of generating and maintaining intracellular tension and force output than NM2C and Myo18a.

Interactomes of NM2A and NM2B versus NM2C and Myo18a suggest divergent functions in developing OLs

Previous studies have shown that the myosins NM2A, NM2B, NM2C and Myo18a bind to actin and are able to oligomerize and form antiparallel bipolar myosin filaments. Of note, *in vivo* Myo18a does not form homotypic filaments, but rather polymerizes with NM2C-based molecules (Billington et al., 2013, 2015). The structural, enzymatic and mechanochemical properties of myosins described above suggest that filaments made out of NM2C and Myh18 are not well suited for processivity along actin filaments and, therefore, may not be able to generate contractile forces as efficiently as NM2A- and NM2B-based filaments. In order to explore this idea, we performed a stringent *in silico* interactome analysis of NM2A, NM2B, NM2C and Myh18a. To gain confidence that a particular physical interaction may exist in the physiological context, we used the EMBL-EBI IntAct database of molecular interactions (https://www.ebi.ac.uk/intact; Orchard et al., 2014) that collects experimental molecular interaction data curated from peer-reviewed scientific publications or directly submitted by the scientific community. Additionally, we used the web service Interactome3D to explore the structural details of protein-protein interaction networks (https://interactome3d.irbbarcelona.org; Mosca et al., 2013), which uses IntAct as one of the source databases. Of note, in order to decrease the degree of artefactual interactions, our analysis did not consider *in silico* predictions of physical protein interactions. Our analysis resulted in the identification of 20, 23, 10 and 11 physical interactors for NM2A, NM2B, NM2C and Myo18a, respectively (Table S1). The significant higher number of interactors for NM2A and NM2B in comparison with NM2C and Myo18a is a reflection of their extensive characterization. Next, we analyzed the expression profile of these interactors in the OL lineage using the Brain-RNA transcriptome database (http://www.brainrnaseq.org), focusing only on those expressed during OL differentiation (Fig. 3A). We identified 17, 18, 4 and 7 interactors for NM2A, NM2B, NM2C and Myo18a, respectively, that were expressed in the OL lineage. Interestingly, we found that the expression of the vast majority of these myosin interactors (71% for NM2A, 88% for NM2B, 50% for NM2C and 71% for Myo18a) decreases during OL differentiation. To further understand the global framework of the myosin interactomes, we performed a functional enrichment heatmap analysis of the interactors using the NIH DAVID bioinformatics functional gene ontology (GO) annotation tool (https://david.ncifcrf.gov; Fig. 3B; Tables S2–S6). Since the expression of NM2A and NM2B decreases during OL differentiation, while NM2C and Myo18a expression increases, and it is possible that they may form heterofilaments *in vivo* as previously described (Billington et al., 2015), we pooled the interactomes of NM2A and NM2B (30 interactors) and compared it with those of NM2C and Myo18a (11 interactors). The GO functional enrichment analysis of these two groups revealed interesting and contrasting findings. Globally, the GO categories for the 30 interactors of NM2A and NM2B suggest that these proteins participate in signaling pathways that link the extracellular environment to the actin cytoskeleton, where NM2A and NM2B may be the downstream effectors of such dynamics. Interesting examples are the small GTPase Rac1 and one of its effectors PAK2, important modulators of cytoskeleton dynamics. In particular, we have previously shown a relevant role of Rac1 in OL myelination (Thurnherr et al., 2006). Previously recognized regulators of NM2 activity, TRPM7 (Clark et al., 2008) and SVIL (Hasegawa et al., 2013), are common interactors of NM2A and NM2B. By contrast, the pooled interactomes of NM2C and Myo18a are enriched in proteins which are expressed mainly in adult brain and converge into functions implicated in cellular trafficking, including transport, secretion and establishment of localization. Some examples include GOLPH3 (Dippold et al., 2009) and Snapin (Tian, 2005). These findings are in agreement with the late upregulation of NM2C and Myo18a in mature OLs, where they may be responsible for regulating myelin production and membrane expansion and deformation.

Temporal and spatial fluctuations of NM2B and NM2C expression correlates with cortical tension and membrane expansion during OL differentiation

To further characterize the spatial and temporal localization of NM2B and NM2C during development, we carried out immunocytochemistry analysis of OPC and OL cultures. Fig. 4A shows the localization of

Journal of Cell Science (2020) 133, jcs232264. doi:10.1242/jcs.232264

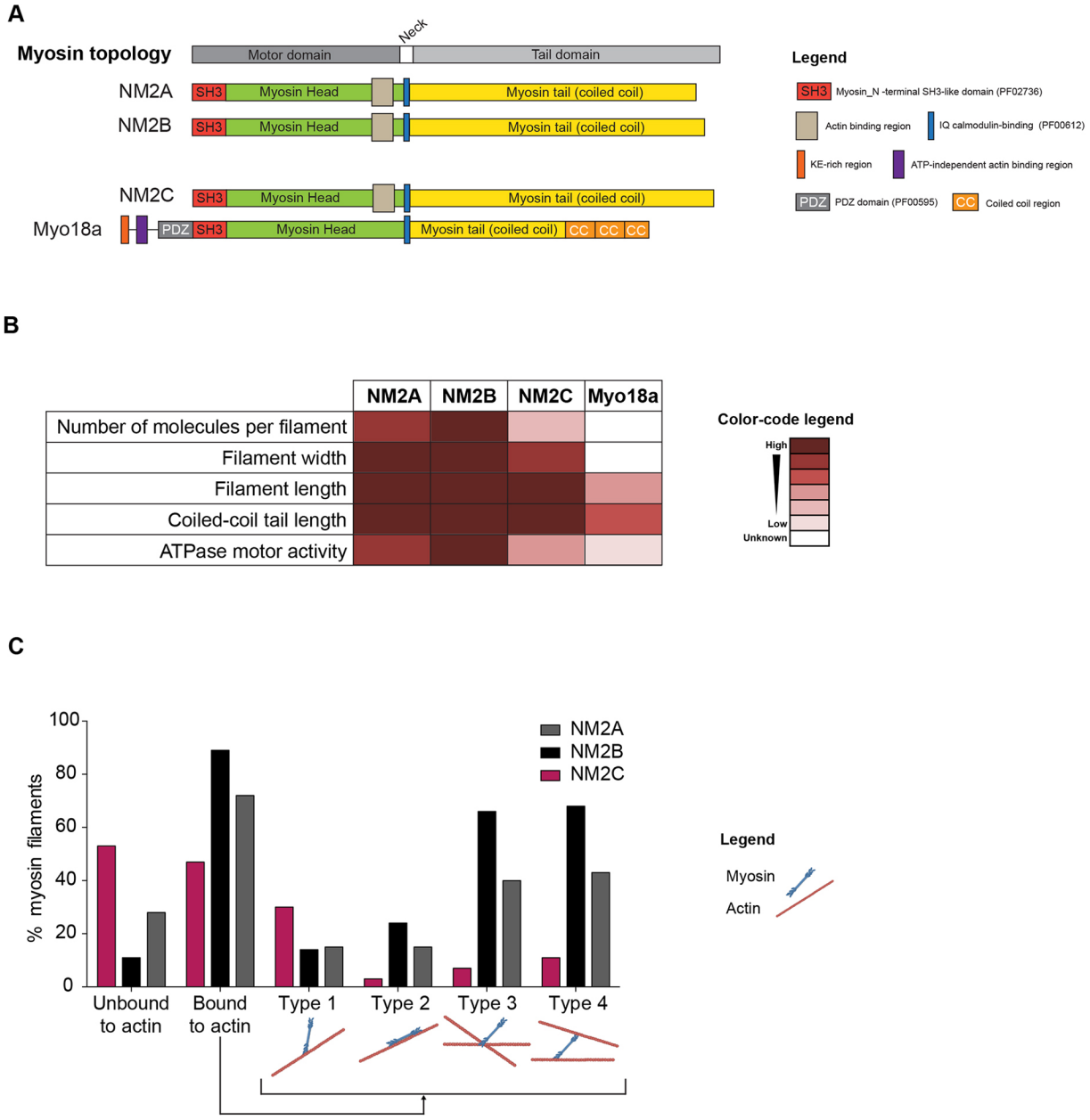

Fig. 2. The phylogenetically and structurally related NM2A, NM2B, NM2C and Myo18a proteins have distinct mechanochemical profiles. (A) Structural domain organization of human myosins NM2A, NM2B, NM2C and Myo18a according to updated information on domain organization and boundaries from the Pfam database (https://pfam.xfam.org), combined with the functional annotation of specific profiles and patterns as described in UniProtKB (https://www.uniprot.org/uniprot). (B) Comparative heatmap representation of several structural and mechanochemical characteristics of human NM2A, NM2B, NM2C and Myo18a myosin bipolar filaments, as quantified by Billington et al. (2013, 2015). (C) Graphical representation of comparative actin binding behavior of NM2 isoforms, as quantified by Billington et al. (2013). Accordingly, plotted is the percentage of all filaments bound or not bound to actin. Bound filaments were classified as type 1 (bound to a single actin filament via one side of the myosin filament), type 2 (bound to a single actin filament by both sides of the myosin filament), type 3 (bound to multiple actin filaments by one side of the myosin filament), or type 4 (bound to multiple actin filaments by both sides of the myosin filament). Of note, types 2, 3, and 4 are not mutually exclusive.

NM2B and NM2C in the OPC soma and the cytoplasm of nascent protrusions. Although both motor proteins are found in the same compartments at this stage, the signal for NM2C extends further distally into the growing processes than that of NM2B. Preliminary time-lapse imaging analysis of NM2B–GFP shows that, at initial differentiation stages, a local decrease of NM2B–GFP levels is observed, which leads to a local decrease in cortex tension favoring branching protrusion. As protrusion emerges, localization of filamentous actin becomes confined to the leading tip and the NM2B released from the cortex is redirected to the tip, as shown in Fig. S2. This localization suggests that unidirectional actin polarization/depolarization dynamics and actin crosslinking by NM2B potentially provides guidance for initial protrusion growth and stability. As OPCs further branch and mature into OLs (Fig. 4B), the differential local distribution of these proteins becomes more apparent, with NM2B mostly localized in the cortical cytoplasm of thicker branches, while NM2C further extends into actin protrusions active in membrane extension. Interestingly, this pattern of NM2C

Journal of Cell Science (2020) 133, jcs232264. doi:10.1242/jcs.232264

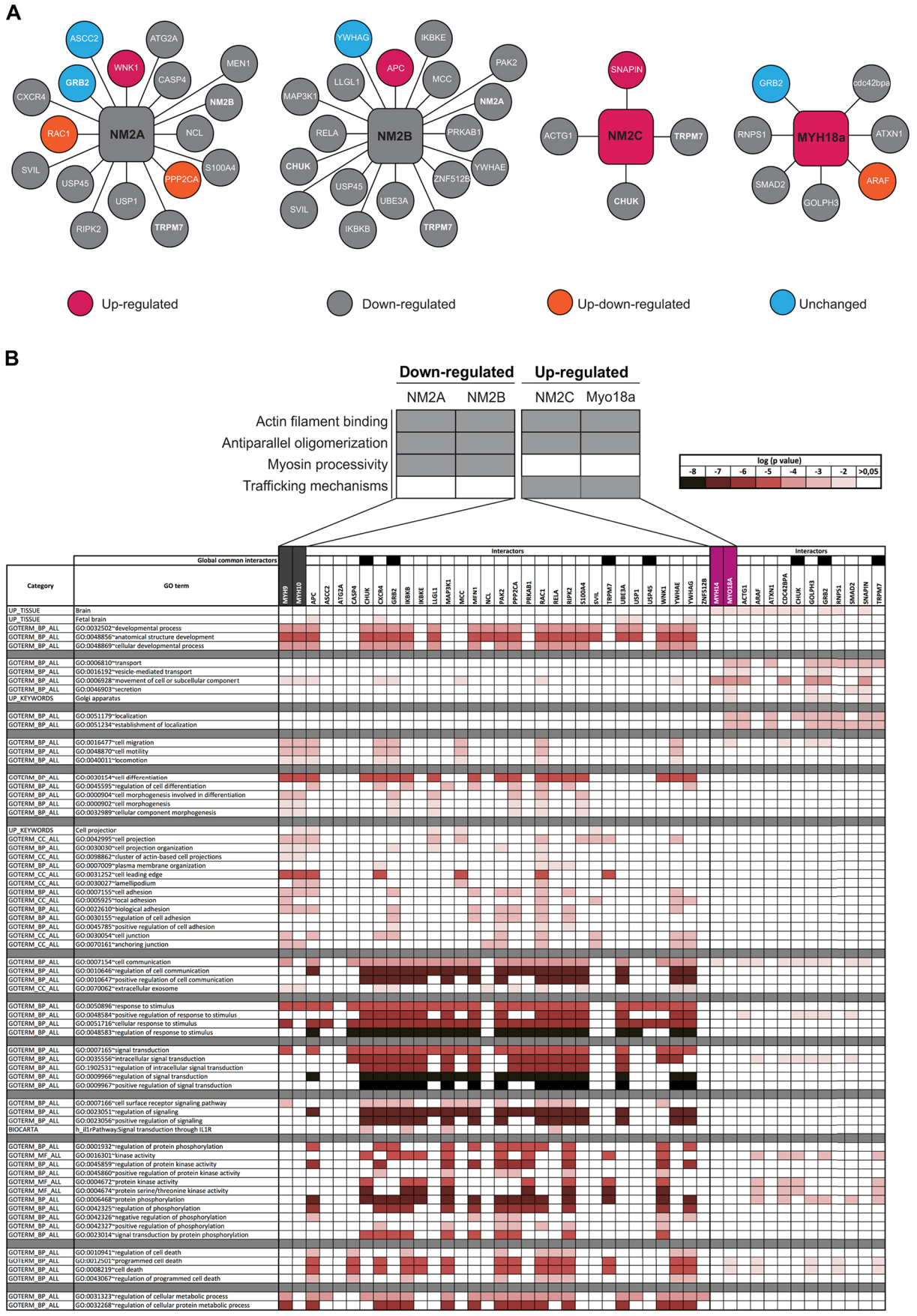

Fig. 3. See next page for legend.

Journal of Cell Science (2020) 133, jcs232264. doi:10.1242/jcs.232264

Fig. 3. Interactomes of NM2A and NM2B versus NM2C and Myo18a suggest divergent functions in developing OL. *In silico* interactome analysis of NM2A, NM2B, NM2C and Myh18a based on the EMBL-EBI IntAct (https://www.ebi.ac.uk/intact) (Orchard et al., 2014) and Interactome3D (https://interactome3d.irbbarcelona.org) (Mosca et al., 2013) databases for protein–protein interactions analysis. All identified interactors are listed in Table S1. The interactors that are expressed in the OL lineage, according to Brain RNAseq (http://www.brainrnaseq.org), are graphically illustrated in A with a color code representative of their temporal expression pattern during OL differentiation: pink, upregulated; gray, downregulated; orange; up- and down-regulated (up-down-regulated); blue, unchanged. (B) Heatmap representation of GO annotation enrichment analysis of pooled NM2A and NM2B versus NM2C and Myo18a interactors using the NIH DAVID bioinformatics functional GO annotation tool (https://david.ncifcrf.gov). A color code was given according to the obtained $\log_{10}$ of the *P* value. The raw data related to this graphical representation is described in Tables S2–S6.

staining is reminiscent of the recently described Golgi outpost compartment, which is characterized as being enriched in microtubules and Myo18a, and is critical for myelination (Fu et al., 2019). Indeed, staining with NM2C, Myo18a and tubulin corroborates that these proteins are found in these outposts in mature OLs (Fig. 4C).

Collectively, the pattern of localization and levels of expression of NM2B, NM2C and Myo18a suggest a model whereby at initial differentiation stages, a local decrease of NM2B leads to local decrease in cortex tension favoring branching protrusion (Fig. 4D). While the global reduction of NM2B leads to cortical tension release, which is a requirement for branching initiation, the speed of protrusion growth and myelin sheet formation is yet dependent on the elasticity of the plasma membrane and the robustness of mechanisms of membrane targeting. The mechanochemical properties and interactomes of NM2C and NM18a suggests their putative involvement in processes of myelin membrane extension and MBP production.

Knockdown of NM2B and NM2C has opposite effects on myelin formation *in vitro*

The differential expression and distribution of NM2B and NM2C in OPC and OL suggest that these two motors might carry out different functions during development. We hypothesize that protrusion growth and local myelin extension and wrapping requires the coordination between plasma membrane elasticity and sustained protein targeting. We have previously reported that global reduction of NM2A and NM2B leads to cortical tension release, and increased OL branching and myelination, while their overexpression inhibits these processes (Wang et al., 2008, 2012). To test whether NM2B and NM2C are involved in different steps of OPC development (branching initiation versus membrane extension), we performed NM2B and NM2C silencing in myelinating co-cultures of OPCs with DRG neurons and examined the effects on myelin formation with shRNA (denoted shNM2B and shNM2C, respectively) (Fig. 5A). Western blots demonstrated the effective knockdown of these proteins in culture (Fig. S3A). Quantitative imaging analysis confirmed that knockdown of NM2B in OPC resulted in a 2-fold increase ($P<0.0001$) in the average number of MBP-positive segments formed in cultures compared to control (Fig. 5B). By contrast, knockdown of NM2C caused a 36% reduction in myelin formation ($P=0.02$) compared to control cultures (Fig. 5B). We found that MBP-positive segments formed in shNM2C-treated cultures appeared abnormal compared to controls and NM2B knockdown cultures (Fig. 5A). In addition, the relative proportion of cultures showing no myelination or less than 40 segments per field (Fig. 5C) was higher in shNM2C (59%) compared to shCtrl (40%) and shNM2B (12%) cultures. By contrast, knockdown of NM2B increases the proportion of fields showing more than 100 myelin segments per field (47%) compared to shCtrl (12%) and shNM2C (6%) (Fig. 5C). Collectively, our results suggest that spatiotemporal fluctuations of NM2B and NM2C control local cortical tension and membrane expansion for initial protrusion growth (NM2B) and subsequent myelin formation (NM2C).

DISCUSSION

OL shape dependency on spatiotemporal patterning of the myosin network

In this study, we have performed an integrative analysis, at the transcriptomic and proteomic level, of all myosin in CNS myelinating glial cells. This work revealed the presence of many myosins in the OL lineage, with some of them not yet functionally characterized. Some of these myosins are expressed in a developmentally coordinated manner, suggesting that they may play distinctive roles during OL differentiation. Here, we highlight seven myosins that have been consistently identified in several independent studies: the three NM2 isoforms and the phylogenetically related Myo18a, and the transport-associated Myo1d, Myo5a and Myo6. While the abundance of *Myh9*, *Myh10* and *Myo5a* transcripts decreases during differentiation, that of *Myo1d*, *Myh14*, *Myo6* and *Myo18a* transcripts increases. Of these, to our knowledge, only a function of NM2C and Myo18a had not previously been described in OL biology.

Our systems biology-oriented analysis revealed members of the NM2 family working as distinctive mechanical regulators of OL cell morphology and differentiation, as proposed in our conceptual model (Fig. 4D). Based on the changes in mRNA and protein expression level of NM2B and NM2C, we propose three stages of the OL development: stage 1 (NM2B is high and NM2C is low), stage 2 (NM2B is reduced and NM2C is elevated), and stage 3 (NM2B is low and NM2C is high). At stage 1, the enrichment of NM2B in the early stages of OL development may contribute to the generation of actomyosin crosslinkage and contractility-based tension. While actin filaments polymerization drives the elongation of OL protrusions (Nawaz et al., 2015; Zuchero et al., 2015) and myosin contractility is released at the protruding edge, NM2B-dependent actomyosin crosslinkage and contractility determines the overall shape of the cell. A non-uniform pattern of NM2B expression at the cortex supports branching initiation, which possibly takes place in regions of decreasing mechanical tension. It can be noted here that the ability of the cortex to elongate (commonly termed as elasticity) is an inverse function of the local mechanical tension. This idea is supported by the observation that NM2B overexpression inhibits OPC branching due to increased cortical tension (Wang et al., 2012). Preliminary data, looking at the local changes in the distribution of cortical NM2B–GFP as OPCs initiate branching (Fig. S2), shows that, as protrusions emerge, localization of filamentous actin becomes confined to the leading tip and the NM2B released from the cortex is redirected to the tip. This redistribution is also in agreement with our previous electron microscopy and immunofluorescence analyses of OPC protrusions (Wang et al., 2012). Subsequently, at stage 2 the global reduction of cortical NM2B expression promotes further branching and protrusion, while relocalization of this motor can be reused for scaffolding of the growing protrusions. Note that at this stage there is no requirement for membrane spreading. The increase in the number of branches is accompanied by the continuous decrease in the NM2B expression, which is not sufficient to promote myelin wrapping as the latter requires increased transport of myelin proteins to the growing myelin sheet. Finally, at stage 3 OL protrusions evolve into myelin-bearing sheets showing low levels of NM2B and higher expression of

Journal of Cell Science (2020) 133, jcs232264. doi:10.1242/jcs.232264

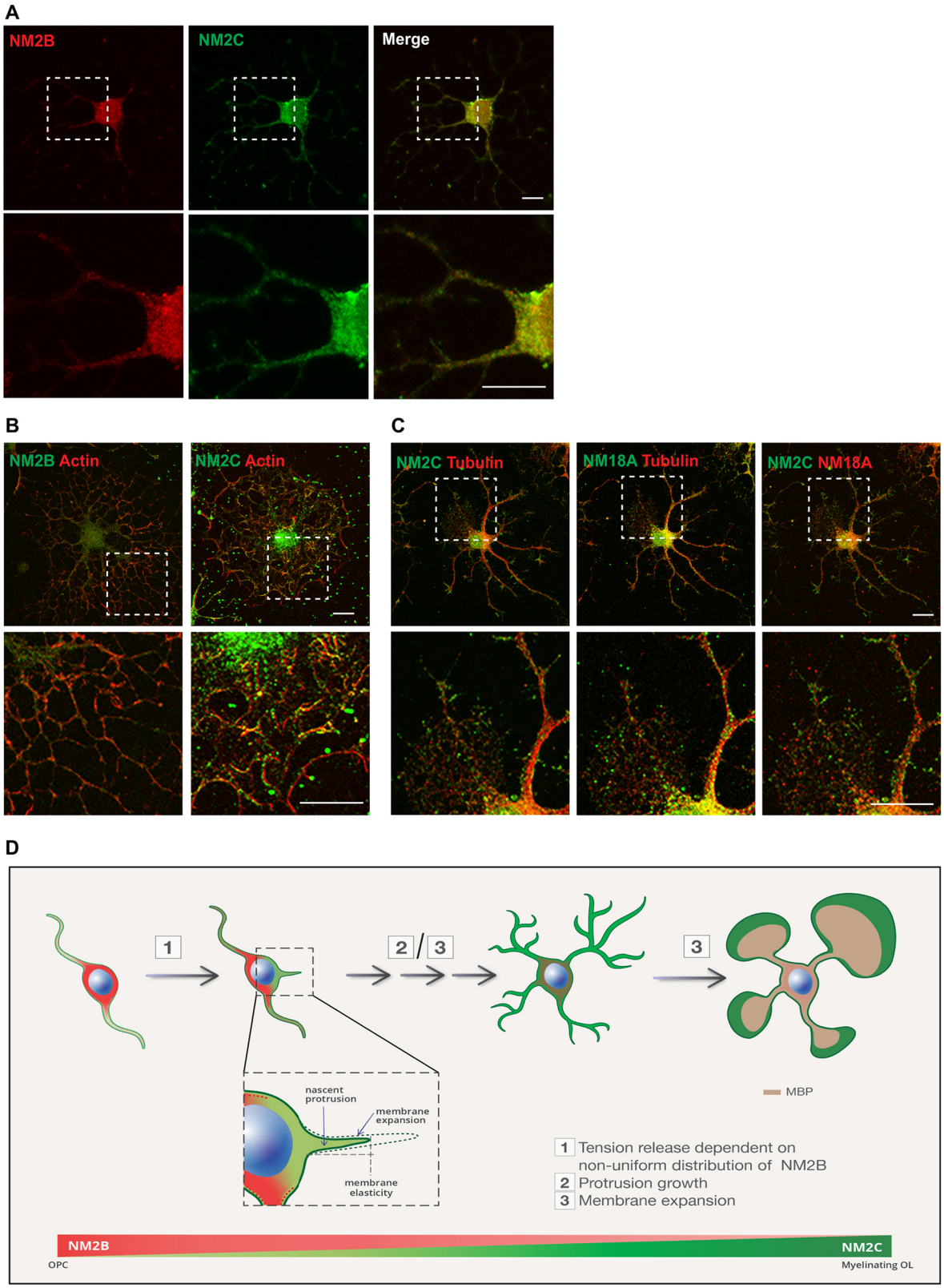

Fig. 4. Spatiotemporal fluctuations of NM2B and NM2C control local cortical tension and membrane expansion for protrusion growth and myelination. (A) NM2B and NM2C expression and localization in nascent OPC protrusions. (B) Localization of NM2B and NM2C in reference to F-actin in mature OL. Magnified images of the boxed area are shown in lower panels. (C) Localization of NM2C and Myo18a in reference to tubulin in mature OL. Magnified images of the boxed area are shown in lower panels. (D) Hypothetical model proposing spatiotemporal fluctuations of NM2B and NM2C in developing OLs that control local cortical tension and membrane expansion for protrusion growth and myelination. Although, not shown in this model for simplicity, the data also predicts that the patterns for NM2A and Myo18 will be similar to those of NM2B and NM2C, respectively. Scale bars: 10 µm.

Journal of Cell Science (2020) 133, jcs232264. doi:10.1242/jcs.232264

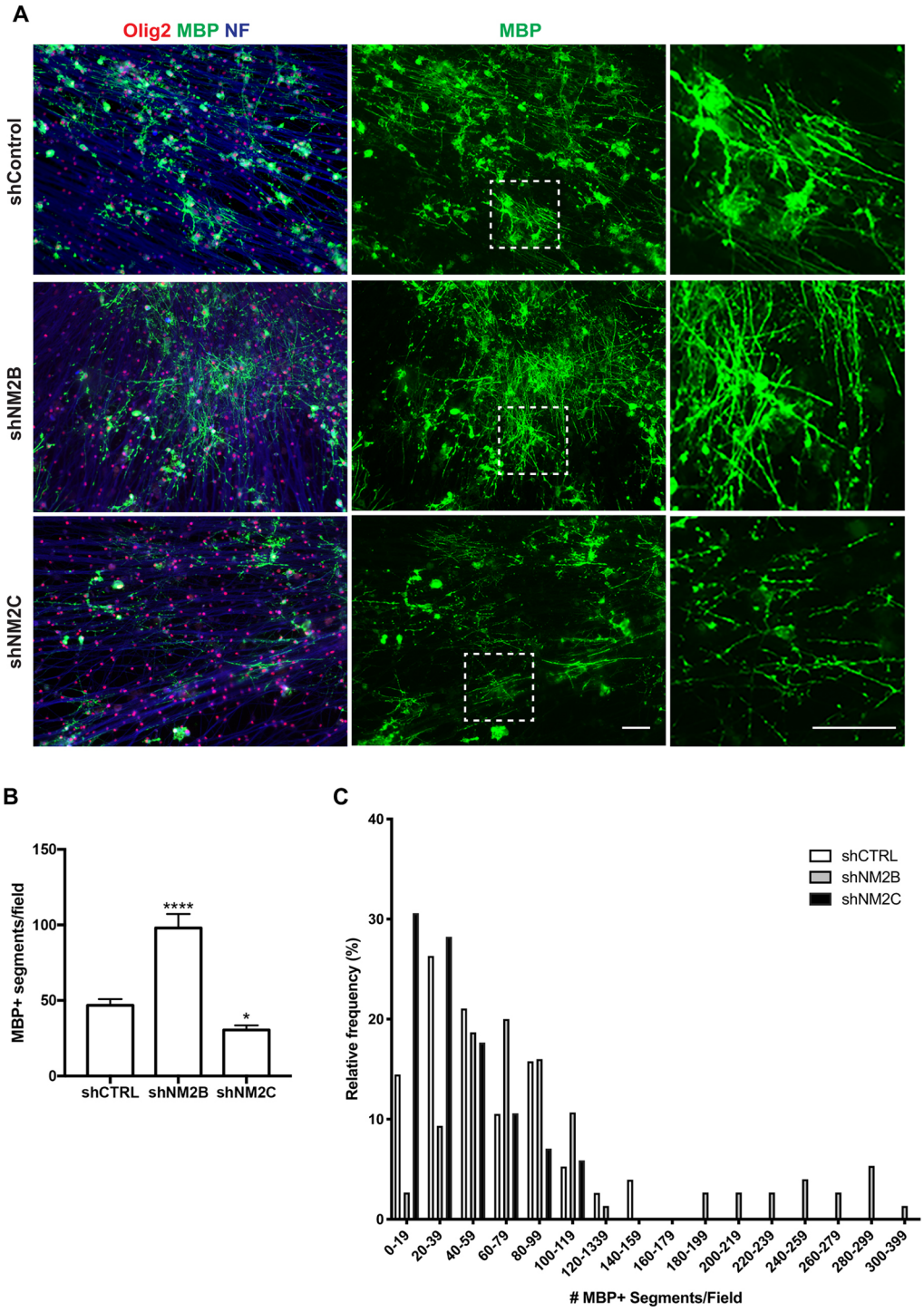

Fig. 5. Knockdown of NM2B and NM2C in OPC–DRG co-cultures have opposite effects in OL differentiation and myelin formation. Knockdown of NM2B and NM2C in OPC co-cultured with DRG neurons. (A) Representative images of 3-week-old myelinating 3D OPC–DRG co-cultures stained for MBP, Olig2 and NF. Co-cultures were infected with a lentiviral vector expressing shRNA against the NM2B, NM2C (shNM2B, shNM2C) or non-targeting sequence (shCtrl). Images on the right are magnified views of the boxed area showing representative myelinated segments for each of the conditions. Scale bars: 20 µm. (B) Quantification of MBP-positive (MBP+) myelin segments in OPC–DRG co-cultures. Data are mean ±s.e.m. values obtained from the quantification of three independent experiments (10–12 fields per culture and three or four cultures per condition/per experiment). *P=0.02 (shCTRL vs shNM2C); ****P<0.0001 (shCTRL vs shNM2B) (Krustal–Wallis non-parametric test followed by Dunn's multiple comparison test). (C) Histogram showing the distribution of MBP+ segments across all experimental conditions.

NM2C. The low expression of NM2B allows further reduction of the cortex tension, which may promote the expansion of the myelin sheet. This condition is necessary but not sufficient, as the cell has to maintain an increased membrane transport to the growing sheet and it is likely secured by the increased expression of NM2C and Myo18a, which are implicated in membrane-bound cargo and trafficking. In agreement with this interpretation, we also found that NM2C and Myo18a colocalized in oligodendrocyte protrusions that are rich in tubulin, and that knockdown of NM2C negatively impacted myelin formation *in vitro*. Furthermore, Myo18a is also found in Golgi outposts, a recently described domain that is needed for proper myelin formation (Fu et al., 2019), and NM2C protein levels are significantly enriched in white matter regions, such as corpus callosum and pons of the adult CNS (Golomb et al., 2004), while NM2B levels are reduced (Cahoy et al., 2008; Wang et al., 2008; Zhang et al., 2014; Marques et al., 2016).

NM2B is an active mechanical switch for intracellular tension control in developing OLs

The integrative analysis of published data and our own results support the emerging idea that the intracellular tension of a developing OL is modulated by varying the levels of the NM2 isoforms in the actomyosin cytoskeleton. Recently, two studies proposed that actin dynamics is the driving force for myelination of

Journal of Cell Science (2020) 133, jcs232264. doi:10.1242/jcs.232264

axons (Nawaz et al., 2015; Zuchero et al., 2015) and that actin, but not actomyosin modulators, influence membrane tension (Nawaz et al., 2015). However, these results were based on measurements in cells treated with blebbistatin, a drug that does not act exclusively on NM2B but may also inhibit NM2C activity (Rauscher et al., 2018; Zhang et al., 2017; Chinowsky et al., 2020 preprint).

The functional enrichment analysis of the pooled interactors of NM2A and NM2B versus NM2C and Myh18a clearly suggest that NM2A and NM2B may have similar functions during OL differentiation. By virtue of their biophysical properties, NM2A and NM2B effectively generate intracellular cell tension and control cell shape to enable the synchronization of various genetic, metabolic and biochemical processes leading to myelin biogenesis. This goes in agreement with the concept that ablation of both NM2A and B *in vitro* accelerates OL differentiation, while their overexpression prevents OL branching and differentiation (Wang et al., 2008, 2012). Although NM2B OL-specific ablation in adult brain also accelerates myelin repair (Rusielewicz et al., 2014), early deletion may have adverse consequences for developmental myelination. Accordingly, it would be relevant to address in the future the phenotype of OPC-specific NM2B ablation in early post-natal brain prior to active myelination. In contrast, NM2C and Myo18a are upregulated later in development (Cahoy et al., 2008; Zhang et al., 2014), at a stage of active elaboration of myelin, suggesting a potential role for NM2C and Myo18a in myelin membrane production. In agreement with this hypothesis, some of the identified interactors of NM2C and Myo18a are involved in cell trafficking and membrane homeostasis. Myelin membrane trafficking involves the assembly of particular components in a spatiotemporal-regulated manner and requires specific sorting and transport mechanisms for delivering myelin components to the sites of membrane growth (Baron and Hoekstra, 2010; Simons et al., 2012). Here, we identified Snapin as one of the potential interactors of NM2C. In chromaffin cells, Snapin is important for Ca^{2+}-dependent exocytosis of large vesicles (Tian, 2005). Although it will be necessary to confirm in the future that NM2C and snapin interact physically in OLs, this finding further supports the hypothesis that NM2C might be involved in mechanisms of membrane trafficking.

It has also been described that NM2 isoforms co-polymerize, both *in vitro* and *in vivo*, to form heterotypic bipolar filaments with hybrid characteristics (Beach et al., 2014). This suggests that the OL during differentiation may fine-tune a broad spectrum of mechanoenzymatic properties with different combinations of myosin heavy chain heterodimers. Additionally, all NM2 isoforms establish heterotypic filaments with Myo18a, which decreases their myosin filament size (Billington et al., 2015). *In vitro*, addition of Myo18a molecules to NM2 filaments interferes with homotypic filament assembly (Billington et al., 2015). Previous studies also demonstrate that NM2A and NM2B filaments have distinct mechanical properties. NM2A holds a higher ATP hydrolysis rate, propelling actin filaments faster, whereas NM2B can exert tension for extended time periods (Vicente-Manzanares et al., 2009; Melli et al., 2018). OLs may therefore adjust the intracellular force output of NM2 filaments for specific functions by altering their composition and/or stoichiometry of their isoforms, possibly together with Myo18a. Future experiments will address the role of this phenomenon on OL differentiation directly, as we have observed that knockdown of Myo18a in purified OLs also decreased the levels of NM2C (data not shown), further suggesting that formation of these heterodimers among myosin motors might add another level of regulation to the cytoskeletal dynamics of myelination.

Intracellular tension can also be modulated based on the ability of class II myosins to induce actin depolymerization. In budding yeast cytokinesis, for example, the major contractile forces results from actin depolymerization mediated by NM2 motor activity and cofilin (Mendes Pinto et al., 2012). In OLs, actin depolymerization is dependent on cofilin/ADF activity (Nawaz et al., 2015). In this context, it is possible that NM2C and Myo18a, which are present in higher abundances in myelinating OL than NM2A and NM2B, are inducing actin depolymerization together with cofilin proteins. Another study proved that active class II myosin motors can quickly 'fluidize' entangled actin networks, decreasing the resistance to cellular deformations (Humphrey et al., 2002). In agreement with this model, we have previously shown that F-actin and phosphorylated MLC2, a read out of active myosin motors, colocalize at the edges of the MBP-positive membranes extended by mature oligodendrocytes in culture (Wang et al., 2008, 2012). This finding indicates that, despite the overall reduction in cortical tension and actomyosin contractily as OLs differentiate, localized activity of myosin motors and actin polymerization/depolymerization act in concert to promote myelin extension.

Overall, this work suggests that intracellular tension generation in a developing OL is crucial for the definition of cell shape and polarization, and this may be acquired by fine-tuning the proportion of NM2 isoforms and the phylogenetically related Myo18a, which associated with actin filaments at each developmental stage. This mechanical output, together with the regulation of actin assembly, will be crucial for the ability of OLs to wrap their myelin sheets around axons. Several examples in other cell and tissue models have nicely illustrated the panoply of possibilities by which different patterns of actomyosin contractility and resulting tension can mold cell and tissue shapes (Heer and Martin, 2017). In the particular case of how developing OL regulate their growth and form, the knowledge of the active molecular mechanisms underlying the resulting forces surely needs to be further characterized in the future.

MATERIALS AND METHODS

Data mining of the OL myosinome

The mRNA and protein expression profile of the myosin network during oligodendrocyte differentiation was cataloged by integrating data from available transcriptomic and proteomic datasets (Cahoy et al., 2008; De Monasterio-Schrader et al., 2012; Zhang et al., 2014; Thakurela et al., 2016; Azevedo et al., 2018) with previous developmental studies of myosin expression (Wang et al., 2012; Yamazaki et al., 2016) during *in vitro*, *ex vivo* and *in vivo* human, mouse and rat developmental oligodendrocyte differentiation. The results from high throughput data presented in the final table derive from the bioinformatics analysis of the original authors.

In silico analysis of myosin structural domains

The information on domain organization and domain boundaries for the selected myosins was retrieved from the Pfam database (https://pfam.xfam.org) and combined with the functional annotation of specific profiles and patterns as described in UniProtKB (https://www.uniprot.org/uniprot).

Interactome analysis of NM2A, NM2B, NM2C and Myh18a

The EMBL-EBI IntAct (https://www.ebi.ac.uk/intact; Orchard et al., 2014) and Interactome3D (https://interactome3d.irbbarcelona.org; Mosca et al., 2013) databases were used to identify direct physical interactors and to explore the structural details of protein–protein interaction networks of NM2A, NM2B, NM2C and Myh18a. The identified interactors were inspected for the temporal expression in the OL lineage as reported in the Brain RNASeq (http://www.brainrnaseq.org; Zhang et al., 2014) and only those were considered for subsequent analysis.

Gene-enrichment and functional annotation analysis was performed to understand the global framework of the NM2A and NM2B versus the NM2C and Myo18a interactomes using the NIH DAVID bioinformatics functional gene ontology (GO) annotation tool (https://david.ncifcrf.gov).

Journal of Cell Science (2020) 133, jcs232264. doi:10.1242/jcs.232264

This enrichment analytic algorithm provided a batch annotation and gene-GO term enrichment analysis to highlight the most relevant gene GO terms, tissue expressions, protein functional domains and bio-pathways associated with a given gene list. The results are displayed in an individual annotation table (Tables S2–S6). We also used the DAVID Functional Annotation Clustering tool to measure the relationships among the annotation terms based on the levels of their co-association genes (Tables S2–S6).

Animal ethics

Vertebrate animal tissue was collected in accordance with the guidelines published in the NIH Guide for the Care and Use of Laboratory Animals for the humane treatment of laboratory animals (Publication No. 85-23, revised 1985). All procedures were approved by Hunter College Institutional Animal Care and Use Committee.

Purified OPC cultures and OPC–DRG myelinating co-cultures

Primary OPCs were purified by immunopanning from mixed glial cultures of postnatal day 1 rat (Sprague Dawley) cerebral cortices as previously described (Wang et al., 2008, 2012). Purified OPCs were seeded onto poly-lysine-coated glass coverslips (20,000–30,000 cells) and maintained in Sato medium (DMEM, 100 µg/ml transferrin, 100 µg/ml BSA, 20 nM progesterone, 100 µM putrescine, 30 nM sodium selenite, 2 mM L-glutamine, 5 µg/ml insulin, 60 µg/ml N-acetyl cysteine and 10 µM forskolin) with 10 ng/ml PDGF and 10 ng/ml bFGF for proliferation or induced to differentiate in Sato medium containing T3 (30 ng/ml). DRG explants were isolated from rat embryonic day 16 spinal cords and plated directly onto glass coverslips coated with Matrigel (BD Biosciences). Explants were kept in NB medium (NB: neurobasal medium, containing 2% B27 supplement, 4 g/l D-glucose, 2 mM L-glutamine and 50 ng/ml NGF) and treated with antimitotic agents to eliminate non-neuronal cells. Explants were allowed to extend a dense neurite network for at least 2–3 weeks before their use in co-culture experiments. OPC–DRG co-cultures were established by seeding freshly purified OPCs (50,000–100,000 cells) onto DRG explants and myelination was induced the following day by addition of 1 µg/ml TrkA-Fc (R&D Systems). Cultures were allowed to myelinate for up to 18–21 days, with fresh medium provided every 2–3 days.

Knockdown of NM2B and NM2C in myelinating OPC–DRG co-cultures

Knockdown of NM2B and NM2C in myelinating OPC–DRG co-cultures was performed using specific shRNAs as previously described (Wang et al., 2008, 2012). Briefly, MISSION® shRNA Lentiviral Transduction Particles were purchased from Sigma. Lentivirus carrying two individual clones (TRCN0000110555 and TRCN0000110558 for NM2B, and TRCN0000110570 and TRCN0000110573 for NM2C) were transduced into OPCs in co-culture with DRG neurons 24 h after seeding. Lentiviral particles were left in culture for 3 days, prior to medium change. In our experience, this approach allows for selective transduction of OPCs over post-mitotic mature neurons and improved OPC survival (Wang et al., 2008, 2012). Co-cultures were maintained in myelinating medium for an additional 18–21 days, prior to fixation and analysis by immunofluorescence. MISSION® pLKO.1-puro non-mammalian shRNA targeting particles were used as controls.

Immunofluorescence

Cell cultures were fixed in 4% PFA and processed for immunocytochemistry as previously described (Wang et al., 2008, 2012). Antibodies used in these studies included: rabbit anti-NM2A, anti-NM2B and anti-NM2C (Cell Signaling, #3403, 3404 and 3405, at 1:200), mouse anti-NM2B (DS Hybridoma Bank, #CMII-25, at 1:100), mouse anti-NM2C (Proteintech, #66825-I-Ig, at 1:4000), rabbit anti-Myo18a (Proteintech, #14611-1-AP, at 1:100), chicken anti-tubulin (Novus, #NB-100-1612, at 1:100), mouse anti-MBP (Sternberger Monoclonal, #SMI94, at 1:200), chicken anti-neurofilament (NF) (Biolegend, #822701, at 1:2000) and rabbit-anti-Olig2 (Abcam, #33427, at 1:1500). Actin-670 (Cytoskeleton, #PHDN1, at 1:100) and secondary antibodies conjugated to Alexa Fluor 647, Rhodamine, Fluorescein, Coumarin or Cyanin 5 were obtained from Jackson Immunoresearch (West Grove, PA) and used at 1:100 dilution. Myelinating co-cultures were examined by epifluorescence on a Leica DMI4000 microscope with a HCX PL FLUOTAR L 20.0×/0.40 NA DRY objective and LAS 1.7.0 software equipped with a digital camera (DFC350FX; Leica). For OPC and OL cultures, images were acquired with a confocal laser scanning microscope (LSM 510; Carl Zeiss, Inc.) using Plan-Apochromat 20×/0.75 NA or Neofluor 40×/1.3 NA oil objectives and LSM software (Carl Zeiss, Inc.).

Cell culture lysates and western blotting

Lysates from OPC and OL cultures were prepared as previously described (Wang et al., 2008), subjected to SDS-PAGE and blotted onto nitrocellulose membranes. Appropriate regions of the blots were cut and incubated with specific antibodies and developed using chemiluminescent substrate (Pierce, Rockford, IL). For estimation of changes in protein levels, X-ray films from two or three independent experiments were scanned, and the relative intensity of each protein band was calculated in ImageJ by dividing the absolute intensity of each protein band (the area of the band by the number of pixels contained in that area) by the absolute intensity of the corresponding actin band.

Rat brain tissue lysates and western blotting

Lysates of rat brains were prepared as previously described (Wang et al., 2008). Briefly, whole-brain homogenates were lysed in a solution containing 1% SDS, 150 mm NaCl, 10 mm EDTA, 1 mm PMSF, 10 µg/ml aprotinin, and 20 µm leupeptin in 50 mm Tris-HCl pH 7.4. Lysates were cleared by centrifugation at 12,000 ***g*** for 10 min. Protein concentrations were determined using the BCA method (Pierce, Rockford, IL). The lysates (10–15 µg total protein per sample) were then subjected to SDS-PAGE and blotted onto nitrocellulose membranes. Appropriate regions of the blots were cut and incubated with specific antibodies and developed using chemiluminescent substrate (Pierce, Rockford, IL). For estimation of changes in protein levels, X-ray films from two or three independent experiments were scanned, and the relative intensity of each protein band was calculated in ImageJ by dividing the absolute intensity of each protein band (the area of the band by the number of pixels contained in that area) by the absolute intensity of the corresponding actin band.

Quantitative image analysis

Image analysis and processing was performed using the freely available NIH ImageJ software, version 2.0.0, and Photoshop CS6 (Adobe). Adjustment of image brightness or contrast was performed in some cases but without misrepresenting data. OPC–DRG myelinating co-cultures were stained with MBP, Olig2 and NF antibodies, and images acquired at low magnification (25×). MBP-positive segments aligned with the NF-positive axon were identified, and counted in micrographs from 10–12 random fields per coverslip (three or four coverslips per condition, per experiment; total of three experiments). Statistical analyses (one-way ANOVA and multiple comparison post-tests) were performed using GraphPad Prism 6 software. For western blots, analyses of band intensity differences between PDGF and 3dT3 conditions were performed using GraphPad Prism 6 software (Krustal–Wallis non-parametric test, followed by Dunn's multiple comparison).

Live imaging of mouse OPCs

Mouse OPCs were prepared as previously described (O'Meara et al., 2011). Briefly, mixed glial cultures were prepared from postnatal day 2 mouse cerebral cortices of transgenic mice (MMRRC_034321-UNC) expressing NM2B–GFP. Cultures were used to generate OPC-enriched glial cultures by separating OPCs from the astrocyte monolayer by orbital shaking, followed by purification through differential adhesion to plastic. Purified OPCs (25,000–30,000 cells) were seeded on poly-lysine/laminin-coated coverslips and kept in proliferating medium containing PDGF and bFGF (10 ng/ml, Peprotech) for the duration of the experiment. Imaging was performed at 37°C on a LeicaDMI-4000B inverted microscope (Leica Microsystems, Buffalo Groove, IL) mounted on a TMC isolation platform (Technical Manufacturing Corporation, Peabody, MA), with a Yokogawa CSU 10 spinning disc head and Hamamatsu C9100–13 ImagEM EMCCD camera. The images were acquired as 16-bit data files, with a 63×/1.4 NA oil objective (0.24 µm/pixel),

using Volocity acquisition (PerkinElmer, Waltham, MA) and processed with ImageJ.

Acknowledgements
The authors acknowledge Inês Mendes Pinto lab members for critical reading of the manuscript, Sandra Maya for the artwork and Zoe Pian for assistance with data acquisition.

Competing interests
The authors declare no competing or financial interests.

Author contributions
Conceptualization: H.S.D., B.R., C.V.M.-V., I.M.P.; Methodology: H.S.D., C.V.M.-V., I.M.P.; Formal analysis: H.S.D., C.V.M.-V., I.M.P.; Investigation: H.S.D., M.M.U., S.M.-R., A.A., A.I., Y.H., H.W., J.B.R., B.R., C.V.M.-V., I.M.P.; Writing - original draft: H.S.D., I.M.P.; Writing - review & editing: H.S.D., C.V.M.-V., I.M.P.; Supervision: C.V.M.-V., I.M.P.; Funding acquisition: C.V.M.-V., I.M.P.

Funding
H.S.D. received financial support by Fundação para a Ciência e Tecnologia (FCT) through a post-doctoral fellowship with the reference SFRH/BPD/90268/2012. S.M.-R. and J.B.R. were supported by FEDER (Fundo Europeu de Desenvolvimento Regional) funds through Norte Portugal Regional Operational Programme (NORTE 2020), under the PORTUGAL 2020 Partnership Agreement in the framework of Project Norte-01-0145-FEDER-000008 (Porto Neurosciences and Neurologic Disease Research Initiative at I3S). C.V.M.-V., M.M.U. and H.W. were supported by the National Institutes of Health (SC1NS000001) and by a Research Centers in Minority Institutions Program grant from the National Center for Research Resources (G12 RR003037). I.M.P. received financial support from the Marie Curie COFUND Programme "NanoTRAINforGrowth", from the European Union's Seventh Framework Programme for research, technological development and demonstration under grant agreement no 600375. This article is a result of the project Nanotechnology based functional solutions (NORTE-01-0145-FEDER-000019), co-financed by Norte Portugal Regional Operational Programme (NORTE 2020), under the PORTUGAL 2020 Partnership Agreement, through the European Regional Development Fund (ERDF). Deposited in PMC for release after 12 months.

Supplementary information
Supplementary information available online at
https://jcs.biologists.org/lookup/doi/10.1242/jcs.232264.supplemental

References

Azevedo, M. M., Domingues, H. S., Cordelières, F. P., Sampaio, P., Seixas, A. I. and Relvas, J. B. (2018). Jmy regulates oligodendrocyte differentiation via modulation of actin cytoskeleton dynamics. *Glia* **66**, 1826-1844. doi:10.1002/glia.23342

Baron, W. and Hoekstra, D. (2010). On the biogenesis of myelin membranes: sorting, trafficking and cell polarity. *FEBS Lett.* **584**, 1760-1770. doi:10.1016/j.febslet.2009.10.085

Beach, J. R., Shao, L., Remmert, K., Li, D., Betzig, E. and Hammer, J. A. (2014). Nonmuscle myosin II isoforms coassemble in living cells. *Curr. Biol.* **24**, 1160-1166. doi:10.1016/j.cub.2014.03.071

Billington, N., Wang, A., Mao, J., Adelstein, R. S. and Sellers, J. R. (2013). Characterization of three full-length human nonmuscle myosin II paralogs. *J. Biol. Chem.* **288**, 33398-33410. doi:10.1074/jbc.M113.499848

Billington, N., Beach, J. R., Heissler, S. M., Remmert, K., Guzik-Lendrum, S., Nagy, A., Takagi, Y., Shao, L., Li, D., Yang, Y. et al. (2015). Myosin 18A coassembles with nonmuscle myosin 2 to form mixed bipolar filaments. *Curr. Biol.* **25**, 942-948. doi:10.1016/j.cub.2015.02.012

Cahoy, J. D., Emery, B., Kaushal, A., Foo, L. C., Zamanian, J. L., Christopherson, K. S., Xing, Y., Lubischer, J. L., Krieg, P. A., Krupenko, S. A. et al. (2008). A transcriptome database for astrocytes, neurons, and oligodendrocytes: a new resource for understanding brain development and function. *J. Neurosci.* **28**, 264-278. doi:10.1523/JNEUROSCI.4178-07.2008

Clark, K., Langeslag, M., Figdor, C. G. and Van Leeuwen, F. N. (2007). Myosin II and mechanotransduction: a balancing act. *Trends Cell Biol.* **17**, 178-186. doi:10.1016/j.tcb.2007.02.002

Clark, K., Middelbeek, J., Dorovkov, M. V., Figdor, C. G., Ryazanov, A. G., Lasonder, E. and Van Leeuwen, F. N. (2008). The α-kinases TRPM6 and TRPM7, but not eEF-2 kinase, phosphorylate the assembly domain of myosin IIA, IIB and IIC. *FEBS Lett.* **582**, 2993-2997. doi:10.1016/j.febslet.2008.07.043

Chinowsky, C. R., Pinette, J. A., Meenderink, L. M. and Tyska, M. J. (2020) Nonmuscle myosin-2 contractility-dependent actin turnover limits the length of epithelial microvilli. *bioRxiv.* doi:10.1101/2020.05.01.072389

De Monasterio-Schrader, P., Jahn, O., Tenzer, S., Wichert, S. P., Patzig, J. and Werner, H. B. (2012). Systematic approaches to central nervous system myelin. *Cell. Mol. Life Sci.* **69**, 2879-2894. doi:10.1007/s00018-012-0958-9

Dippold, H. C., Ng, M. M., Farber-Katz, S. E., Lee, S.-K., Kerr, M. L., Peterman, M. C., Sim, R., Wiharto, P. A., Galbraith, K. A., Madhavarapu, S. et al. (2009). GOLPH3 Bridges phosphatidylinositol-4- phosphate and actomyosin to stretch and shape the golgi to promote budding. *Cell* **139**, 337-351. doi:10.1016/j.cell.2009.07.052

Domingues, H. S., Cruz, A., Chan, J. R., Relvas, J. B., Rubinstein, B. and Pinto, I. M. (2018). Mechanical plasticity during oligodendrocyte differentiation and myelination. *Glia* **66**, 5-14. doi:10.1002/glia.23206

Fu, M.-M., Mcalear, T. S., Nguyen, H., Oses-Prieto, J. A., Valenzuela, A., Shi, R. D., Perrino, J. J., Huang, T.-T., Burlingame, A. L., Bechstedt, S. et al. (2019). The Golgi outpost protein TPPP nucleates microtubules and is critical for myelination. *Cell* **179**, 132-146.e14. doi:10.1016/j.cell.2019.08.025

Furusawa, T., Ikawa, S., Yanai, N. and Obinata, M. (2000). Isolation of a novel PDZ-containing myosin from hematopoietic supportive bone marrow stromal cell lines. *Biochem. Biophys. Res. Commun.* **270**, 67-75. doi:10.1006/bbrc.2000.2377

Golomb, E., Ma, X., Jana, S. S., Preston, Y. A., Kawamoto, S., Shoham, N. G., Goldin, E., Conti, M. A., Sellers, J. R. and Adelstein, R. S. (2004). Identification and characterization of nonmuscle myosin II-C, a new member of the myosin II family. *J. Biol. Chem.* **279**, 2800-2808. doi:10.1074/jbc.M309981200

Hasegawa, H., Hyodo, T., Asano, E., Ito, S., Maeda, M., Kuribayashi, H., Natsume, A., Wakabayashi, T., Hamaguchi, M. and Senga, T. (2013). The role of PLK1-phosphorylated SVIL in myosin II activation and cytokinetic furrowing. *J. Cell Sci.* **126**, 3627-3637. doi:10.1242/jcs.124818

Heer, N. C. and Martin, A. C. (2017). Tension, contraction and tissue morphogenesis. *Development* **144**, 4249-4260. doi:10.1242/dev.151282

Heissler, S. M. and Sellers, J. R. (2016). Kinetic adaptations of myosins for their diverse cellular functions. *Traffic* **17**, 839-859. doi:10.1111/tra.12388

Humphrey, D., Duggan, C., Saha, D., Smith, D. and Käs, J. (2002). Active fluidization of polymer networks through molecular motors. *Nature* **416**, 413-416. doi:10.1038/416413a

Isogawa, Y., Kon, T., Inoue, T., Ohkura, R., Yamakawa, H., Ohara, O. and Sutoh, K. (2005). The N-terminal domain of MYO18A has an ATP-insensitive actin-binding site. *Biochemistry* **44**, 6190-6196. doi:10.1021/bi0475931

Kippert, A., Fitzner, D., Helenius, J. and Simons, M. (2009). Actomyosin contractility controls cell surface area of oligodendrocytes. *BMC Cell Biol.* **10**, 71. doi:10.1186/1471-2121-10-71

Laursen, L. S., Chan, C. W. and Ffrench-Constant, C. (2011). Translation of myelin basic protein mRNA in oligodendrocytes is regulated by integrin activation and hnRNP-K. *J. Cell Biol.* **192**, 797-811. doi:10.1083/jcb.201007014

Li, J., Lu, Q. and Zhang, M. (2016). Structural basis of cargo recognition by unconventional myosins in cellular trafficking. *Traffic* **17**, 822-838. doi:10.1111/tra.12383

Marques, S., Zeisel, A., Codeluppi, S., Van Bruggen, D., Mendanha Falcao, A., Xiao, L., Li, H., Haring, M., Hochgerner, H., Romanov, R. A. et al. (2016). Oligodendrocyte heterogeneity in the mouse juvenile and adult central nervous system. *Science* **352**, 1326-1329. doi:10.1126/science.aaf6463

Melli, L., Billington, N., Sun, S. A., Bird, J. E., Nagy, A., Friedman, T. B., Takagi, Y. and Sellers, J. R. (2018). Bipolar filaments of human nonmuscle myosin 2-A and 2-B have distinct motile and mechanical properties. *eLife* **7**, e32871. doi:10.7554/eLife.32871

Mendes Pinto, I., Rubinstein, B., Kucharavy, A., Unruh, J. R. and Li, R. (2012). Actin depolymerization drives actomyosin ring contraction during budding yeast cytokinesis. *Dev. Cell* **22**, 1247-1260. doi:10.1016/j.devcel.2012.04.015

Mosca, R., Céol, A. and Aloy, P. (2013). Interactome3D: adding structural details to protein networks. *Nat. Methods* **10**, 47-53. doi:10.1038/nmeth.2289

Nawaz, S., Sánchez, P., Schmitt, S., Snaidero, N., Mitkovski, M., Velte, C., Brückner, B. R., Alexopoulos, I., Czopka, T., Jung, S. Â. Y. et al. (2015). Actin filament turnover drives leading edge growth during myelin sheath formation in the central nervous system. *Dev. Cell* **34**, 139-151. doi:10.1016/j.devcel.2015.05.013

O'Meara, R. W., Ryan, S. D., Colognato, H., and Kothary, R. (2011). Derivation of enriched oligodendrocyte cultures and oligodendrocyte/neuron myelinating co-cultures from post-natal murine tissues. *JoVE-J. Vis. Exp.* **54**, 3324. doi:10.3791/3324

Orchard, S., Ammari, M., Aranda, B., Breuza, L., Briganti, L., Broackes-Carter, F., Campbell, N. H., Chavali, G., Chen, C., del-Toro, N. et al. (2014). The MIntAct project - IntAct as a common curation platform for 11 molecular interaction databases. *Nucleic Acids Res.* **42**, D358-D363. doi:10.1093/nar/gkt1115

Peckham, M. (2011). Coiled coils and SAH domains in cytoskeletal molecular motors. *Biochem. Soc. Trans.* **39**, 1142-1148. doi:10.1042/BST0391142

Rauscher, A. Á., Gyimesi, M., Kovács, M., Málnási-Csizmadia, A. (2018). Targeting Myosin by Blebbistatin Derivatives: Optimization and Pharmacological Potential. *Trends Biochem. Sci.* **43**, 700-713. doi:10.1016/j.tibs.2018.06.006

Rusielewicz, T., Nam, J., Damanakis, E., John, G. R., Raine, C. S. and Melendez-Vasquez, C. V. (2014). Accelerated repair of demyelinated CNS lesions in the absence of non-muscle myosin IIB. *Glia* **62**, 580-591. doi:10.1002/glia.22627

Sebé-Pedrós, A., Grau-Bové, X., Richards, T. A. and Ruiz-Trillo, I. (2014). Evolution and classification of myosins, a paneukaryotic whole-genome approach. *Genome Biol. Evol.* **6**, 290-305. doi:10.1093/gbe/evu013

Sellers, J. R. (2000). Myosins: a diverse superfamily. *Biochim. Biophys. Acta Mol. Cell Res.* **1496**, 3-22. doi:10.1016/S0167-4889(00)00005-7

Simons, M., Snaidero, N. and Aggarwal, S. (2012). Cell polarity in myelinating glia: From membrane flow to diffusion barriers. *Biochim. Biophys Acta - Mol. Cell Biol. L.* **1821**, 1146-1153. doi:10.1016/j.bbalip.2012.01.011

Sloane, J. A. and Vartanian, T. K. (2007). Myosin Va controls oligodendrocyte morphogenesis and myelination. *J. Neurosci.* **27**, 11366-11375. doi:10.1523/JNEUROSCI.2326-07.2007

Song, J., Goetz, B. D., Baas, P.W. and Duncan, I. D. (2001). Cytoskeletal reorganization during the formation of oligodendrocyte processes and branches. *Mol. Cell. Neurosci.* **17**, 624-636. doi:10.1006/mcne.2001.0974

Stam, S., Alberts, J., Gardel, M. L. and Munro, E. (2015). Isoforms confer characteristic force generation and mechanosensation by myosin II filaments. *Biophys. J.* **108**, 1997-2006. doi:10.1016/j.bpj.2015.03.030

Tan, I., Yong, J., Dong, J. M., Lim, L. and Leung, T. (2008). A tripartite complex containing MRCK modulates lamellar actomyosin retrograde flow. *Cell* **135**, 123-136. doi:10.1016/j.cell.2008.09.018

Thakurela, S., Garding, A., Jung, R. B., Müller, C., Goebbels, S., White, R., Werner, H. B. and Tiwari, V. K. (2016). The transcriptome of mouse central nervous system myelin. *Sci. Rep.* **6**, 25828. doi:10.1038/srep25828

Thurnherr, T., Benninger, Y., Wu, X., Chrostek, A., Krause, S. M., Nave, K.-A., Franklin, R. J. M., Brakebusch, C., Suter, U. and Relvas, J. B. (2006). Cdc42 and Rac1 signaling are both required for and act synergistically in the correct formation of myelin sheaths in the CNS. *J. Neurosci.* **26**, 10110-10119. doi:10.1523/JNEUROSCI.2158-06.2006

Tian, J.-H. (2005). The role of Snapin in Neurosecretion: snapin knock-out mice exhibit impaired calcium-dependent exocytosis of large dense-core vesicles in chromaffin cells. *J. Neurosci.* **25**, 10546-10555. doi:10.1523/JNEUROSCI.3275-05.2005

Vicente-Manzanares, M., Ma, X., Adelstein, R. S. and Horwitz, A. R. (2009). Non-muscle myosin II takes centre stage in cell adhesion and migration. *Nat. Rev. Mol. Cell Biol.* **10**, 778-790. doi:10.1038/nrm2786

Wang, H., Tewari, A., Einheber, S., Salzer, J. L. and Melendez-Vasquez, C. V. (2008). Myosin II has distinct functions in PNS and CNS myelin sheath formation. *J. Cell Biol.* **182**, 1171-1184. doi:10.1083/jcb.200802091

Wang, H., Rusielewicz, T., Tewari, A., Leitman, E. M., Einheber, S. and Melendez-Vasquez, C. V. (2012). Myosin II is a negative regulator of oligodendrocyte morphological differentiation. *J. Neurosci. Res.* **90**, 1547-1556. doi:10.1002/jnr.23036

Wilson, R. and Brophy, P. J. (1989). Role for the oligodendrocyte cytoskeleton in myelination. *J Neurosci. Res.* **22**, 439-448. doi:10.1002/jnr.490220409

Yamazaki, R., Ishibashi, T., Baba, H. and Yamaguchi, Y. (2014). Unconventional myosin ID is expressed in myelinating oligodendrocytes. *J. Neurosci. Res.* **92**, 1286-1294. doi:10.1002/jnr.23419

Yamazaki, R., Ishibashi, T., Baba, H. and Yamaguchi, Y. (2016). Knockdown of unconventional myosin ID expression induced morphological change in oligodendrocytes. *ASN Neuro* **8**, 175909141666960. doi:10.1177/1759091416669609

Yamazaki, R., Ishibashi, T., Baba, H. and Yamaguchi, Y. (2017). Expression of unconventional myosin VI in oligodendrocytes. *Neurochem. Res.* **42**, 3372-3381. doi:10.1007/s11064-017-2377-7

Zalc, B. (2016). The acquisition of myelin: an evolutionary perspective. *Brain Res.* **1641**, 4-10. doi:10.1016/j.brainres.2015.09.005

Zhang, H. M., Ji, H. H., Ni, T., Ma, R. N., Wang, A. and Li, X. D. (2017). Characterization of Blebbistatin Inhibition of Smooth Muscle Myosin and Nonmuscle Myosin-2. *Biochemistry.* **56**, 4235-4243. doi:10.1021/acs.biochem.7b00311

Zhang, Y., Chen, K., Sloan, S. A., Bennett, M. L., Scholze, A. R., O'keeffe, S., Phatnani, H. P., Guarnieri, P., Caneda, C., Ruderisch, N. et al. (2014). An RNA-sequencing transcriptome and splicing database of glia, neurons, and vascular cells of the cerebral cortex. *J. Neurosci.* **34**, 11929-11947. doi:10.1523/JNEUROSCI.1860-14.2014

Zuchero, J. B., Fu, M.-, Sloan, S. A., Ibrahim, A., Olson, A., Zaremba, A., Dugas, J. C., Wienbar, S., Caprariello, A. V., Kantor, C. et al. (2015). CNS myelin wrapping is driven by actin disassembly. *Dev. Cell* **34**, 152-167. doi:10.1016/j.devcel.2015.06.011

S1 Figure

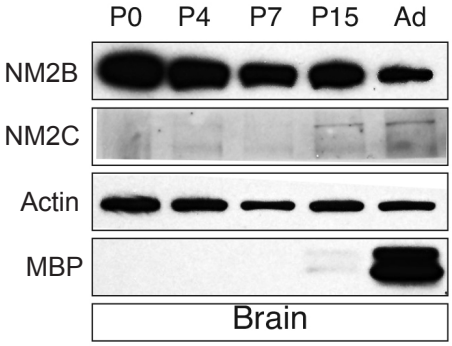

Figure S1 – Differential expression of NM2B and NM2C during *in vivo* myelination. Western blot from whole CNS rat brain at different time points of developmental myelination to analyze bulk protein expression levels of NM2B (down-regulation) and NM2C (up-regulation) and their correlation with MBP expression.

S2 Figure

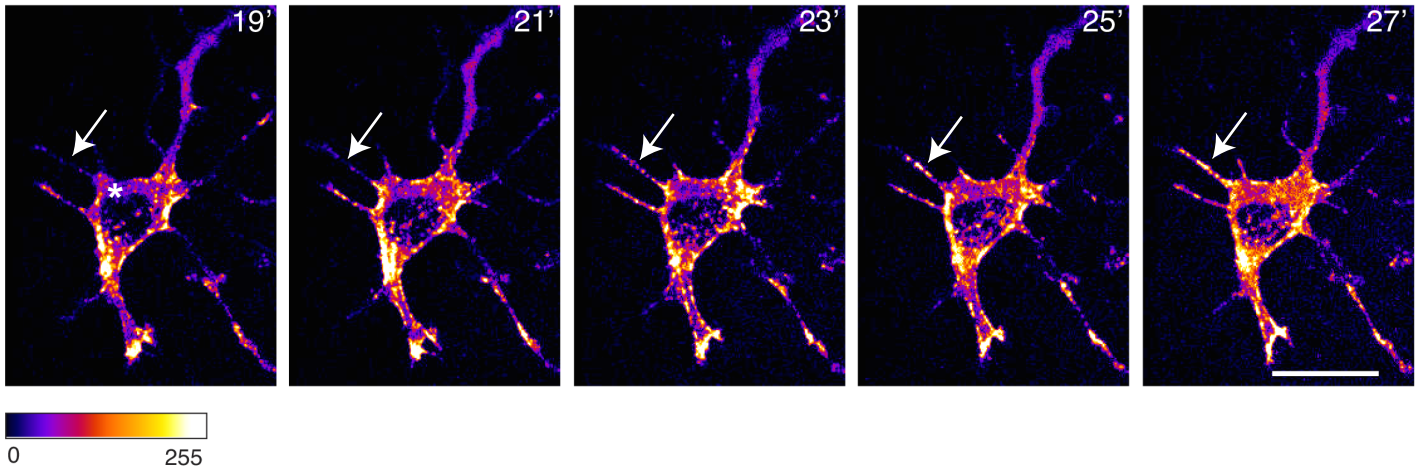

Figure S2 - Dynamic changes on NM2B-GFP subcellular distribution in OPC nascent protrusions. Time-lapse images of OPC cultures purified from transgenic NM2B-GFP mice. Images were acquired using a 63x oil-objective for a period of 35 min. Selected frames clearly show re-localization of NM2B signal from the cortex to the protrusions. Scale bar corresponds to 20µm.

S3 Figure

A

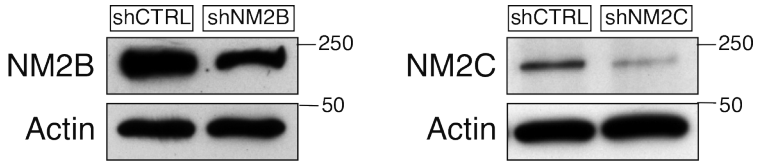

Figure S3 – Validation of knockdown efficiency. Western blots showing the decrease of NM2B and NM2C protein expression in OPC cultures transduced with lentiviral particles. Extracts were prepared 3 days after transduction. Data related to **Figure 5**.

Table S1 – Global NM2A, NM2B, NM2C and Myo18a interactomes. Raw data related to **Figure 3A**.

Click here to Download Table S1

Table S2 - Functional enrichment heatmap analysis of pooled NM2A/NM2B vs. NM2C/Myo18a interactors using DAVID bioinformatics tool. Raw data related to **Figure 3B**.

Click here to Download Table S2

Table S3 - NM2A/NM2B Functional Annotation Table, using DAVID bioinformatics tool. Raw data related to **Figure 3B**.

Click here to Download Table S3

Table S4 - NM2C/Myo18a Functional Annotation Table, using DAVID bioinformatics tool. Raw data related to **Figure 3B**.

Click here to Download Table S4

Table S5 - NM2A/NM2B Functional Annotation Clustering, using DAVID bioinformatics tool. Raw data related to **Figure 3B**.

Click here to Download Table S5

Table S6 - NM2C/Myo18a Functional Annotation Clustering, using DAVID bioinformatics tool. Raw data related to **Figure 3B**.

Click here to Download Table S6